International Journal of
INTELLIGENT SYSTEMS AND APPLICATIONS IN ENGINEERING
ISSN:2147-6799 www.ijisae.org Original Research Paper

A Novel Medical Image Fusion Method Using Modified Grey Wolf Optimization in Wavelet Transform Domain

[1]Sreelekshmi A. N., [2]N. Sujatha, [3]Latha NarayananValli

Submitted: 04/05/2024 **Revised**: 17/06/2024 **Accepted**: 24/06/2024

Abstract: Medical image fusion has emerged as a crucial tool in modern healthcare, facilitating comprehensive analysis by integrating different image modalities into a single image. This fused image aids physicians in disease diagnosis and treatment planning. Despite the advancements in fusion methodologies, effectively merging medical images without compromising any information remains a significant challenge, leading to the exploration of novel methodologies. This study introduces a novel approach for image fusion that utilizes the Modified Grey Wolf Optimization (MGWO) algorithm and the Enhanced Wavelet Transform (EWT). Source images are processed using EWT to extract high- and low-frequency subbands. The low-frequency subbands are fused using the Local Energy Maxima (LEM) criterion.High-frequencysubbandsundergo denoisingusingan enhanced thresholding technique, followed by the application of MGWO to determine adaptive weights for integrating high-frequency subbands for a medical image fusion. An inverse wavelet transform reconstructs the fused image from fused low-frequency and high-frequency subbands. Numerous datasets are tested, wherein the quantitative and qualitative evaluation confirms the effectiveness of the proposed method. Compared to standard models, the proposed technique performed well in experiments, highlighting its potential for enhancing medical image fusion and advancing diagnostic capabilities in healthcare applications.

Keywords: *Medical image fusion, Enhanced wavelet transform, Modified grey wolfoptimization algorithm, Local energy maxima, Computed tomography.*

1. Introduction

Biomedical imaging system plays a pivotal role inthe non-invasive monitoring and diagnosis of internal body organs. These systems are essential for detecting a range of diseases, including tumors, cancer, tuberculosis, diabetic foot ulcers, and COVID-19. Several methods for understanding the interior body organ are shown in these images[1]. To get particular medical data on an organ, there are several imaging methods accessible [2], including Computed Tomography (CT), Magnetic Resonance Imaging (MRI), sonography, X-ray, Positron Emission Tomography (PET), and Single Photo Emission Computed Tomography (SPECT). Each modality offers unique insights into different aspects of the body. For example, a CT scan excels in making skeletal structures, aiding in the detection of internal injuries, broken bones, blood clots, and brain tumors. On the other hand, MRI specializes in capturing soft tissue characteristics of organs like the pancreas, liver, and abdomen. Metabolism information is gleaned through PET and SPECT scans. However, no single modality can offer significant and accurate information [3].

To diagnose a disease, physicians typically analyze dense structures and soft tissue separately, which tends to be tedious and time-consuming. Therefore, medical image is desirable. To tackle such an issue and enhance diagnostic accuracy, image fusion is employed. Image fusion merges complementary information from multiple imaging modalities, resulting in images that contain richer data and are more effective for disease diagnosis [4]. Furthermore, fused imagesnot only reduce the time required for analysis but also improve overall accuracy, facilitating more efficient disease diagnosis and surgical planning [5].There are several levels at which image fusion may be used, including pixel-based [6], feature-based [7], and decision-based [8]. While feature-level fusion gathers and unifies important characteristics from each modality, such as edges, forms, and boundaries, pixel-level fusion combines information from the input directly. A high-level summary showing the objective is provided via decision-level fusion.

Despite the introduction of numerous medical image fusion methods, there remains room for improvement in the quality of fused images. Some methods produce unsatisfactory results, especially around the boundaries

[1] *Assistant Professor, Department of Computer Science, SreeAyyappa College, Eramallikkara, Chengannur, Kerala, India.*
sree.an1989@gmail.com
[2]*Associate Professor, P.G & Research Department of Computer Science, Sri Meenakshi Govt. Arts College for Women (Autonomous), Madurai Kamaraj University, Madurai Tamilnadu ,India*
sujamurugan@gmail.com
[3]*Vice President, Standard Chartered Global Business Services SdnBhd, Kuala Lumpur, Malaysia*
latha.nv@gmail.com

of areas defined by the original images, which may result in an inaccurate diagnosis. Fused images may suffer from poor contrast, noise, and poor quality. To tackle these shortcomings, this paper presents an innovative framework to fuse medical images by employing Enhanced Wavelet Transform (EWT) and a metaheuristic algorithm. The proposed method utilizes MGWO to optimize weights for fusing subbands, effectively transferring source image textural properties to the combined image. Using a fitness function, the source image and fused image peak signal-to-noise ratio (PSNR) is maximized. Weights are adaptive and calculated separately for each high-frequency sub-band, improving fusion flexibility and accuracy. Additionally, the Local Energy Maxima (LEM)low-frequency bands are fused using a technique that takes into account the source images' maximum energy.The proposed method is evaluated using a variety of images gathered from the Brain atlas comprising carious CT and MRI images [9]. The inverse transform of the fused low-frequency and high-frequency sub-bands gives the fused image.The proposed method is analyzed both quantitatively and qualitatively and compared with other benchmark methods. The following are some significant contributions made using the suggested method:

- To address the drawbacks of pixel-level fusion and include the benefits of both approaches in the fusion process, a novel fusion method combining EWT and MGOA is developed.
- The low- and high-frequency subbands of the source images are retrieved using the suggested method's EWT. The suggested approach does away with the negative aspects of pixel-level fusion, namely noise sensitivity and blurring effects, with the use of enhanced thresholding.
- To integrate high-frequency sub-bands and retain information from both source images in the fused image, an MGOA is utilized to generate adaptive weights.
- Using the LEM fusion rule, the proposed method preserves the required complementary results such as edges, borders, and texture information in the low-frequency subbands.
- Compare the performance of the EWT-MGWO with other methods.

The remaining parts of the paper are as follows: An overview of related studies is presented in Section 2. The suggested image fusion approaches are explained in Section 3. Section 4 presents experimental findings and remarks. Section 5 covers the conclusion and future work.

2. Literature Review

In recent decades, a wide range of image fusion techniques have been created [3], [10],[11]. Transformational and spatial image fusion methods are available. In their original spatial domain, spatial domain algorithms integrate source image pixels. Spatial domains are easy to implement. However, these methods might not effectively handle noise present in the input image, and brighteners distortion.Transform domain methods convert source images to a different domain using techniques like Fourier Transform (FT), wavelet, and pyramid. Transform domain-based methods provide better image quality of fused images.

Kaur and Kaur [12]implemented Independent Component Analysis (ICA) and wavelet to create an image fusion technique. Wavelet transform was used to separate the source images into high-frequency and low-frequency subbands. Independent Component Analysis (ICA) based fusion was done. They found that the ICA-based fusion enhances the quality of the fused image. However, ICA-based fusion is sensitive to noise.

Bhateja et al.[13] devised a transform domain-based method for medical image fusion. Using the Stationary Wavelet Transform (SWT), the source images were divided into their approximate and detailed subbands. Following the use of inverse SWT, these coefficients were aggregated by PCA. The acquired images were converted utilizing the maximal fusion rule to fuse the coefficients after the images were changed using a non-sampled contourlet Transform (NSCT). Lowering the combined image's spatial resolution.

In [14], Ullah et al. proposed a non-down sampling shear wave transform-based technique for image fusion. Using this technique, by extracting important feature information from the source images, the fused image's quality was enhanced. Nevertheless, this approach is unable to reflect edge data.

Li and Li introduced a brain image fusion technique based on erroneous texture reduction [15]. This method involved a two-layer decomposition process to create low and high-frequency subbands. To easily detect high-frequency subband details, a feature identification technique based on gradient difference and entropy was presented. A random walk was used to combine coefficients. This approach is tested only on brain images, necessitating further investigation.

Kumar et al.[16] implemented a multimodal image fusion technique by integrating Discrete CurveletTransform (DCuT) and metaheuristic algorithm.Using Fast DCuT, the scientists separated the original images into high- and low-frequency subbands. The low-frequency components were combined through

an averaging fusion rule, while the high-frequency components were merged using fuzzy entropy optimized by the Adaptive Electric Fish Optimization Algorithm (AEFOA). While this method yielded improved results, it is noted for its drawback of introducing distortion in the resulting fused image.

Asha et al. [17] combined Chaotic Grey Wolf Optimization (CGWO) and NSST bands to fuse medical images. In this approach, source images were divided into low-frequency and high-frequency using NSST. Max Fusion Rule was used to fuse low-frequency bands, while CGWO was used to fuse high-frequency bands.

Tawfik et al. [18] suggested a hybrid approach that combined Principal Component Analysis (PCA) with the Discrete Wavelet Transform (DWT). Input images were divided into approximation and detailed subbands. Approximation bands were fused using the max rule while detailed bands were fused using PCA.

Kaur and Singh [19] implemented a deep neural network for medical image fusion. Source images were divided into subbands via Non-subsampled Contourlet Transform (NSCT). Following this, to calculate features from source images, Xception was used. Optimal features were chosen using a differential evolution algorithm.

Polinati et al. [20] investigated the power of Variational Mode Decomposition (VMD) in medical image fusion. Input images were divided into multiple Intrinsic Mode Functions (IMFs) and then fused using the LEM fusion rule. Shilpa et al. [21] used the Enhanced JAYA (EJAYA) optimization algorithm for merging medical images in the NSST domain. Using NSST to separate medical images into low- and high-frequency bands, weights optimized by the EJAYA algorithm were then used to fuse the images.

3. Proposed Methodology

Enhancing the features of both soft and hard tissues in the fused image is the main driving force behind the suggested approach. The suggested technique is to enhance the quality of the fused images while preserving all relevant details from the original images. To achieve this, a blend of EWT and MGOA is employed, leveraging the strengths of each technique while mitigating the weakness of Discrete Wavelet Transform (DWT).

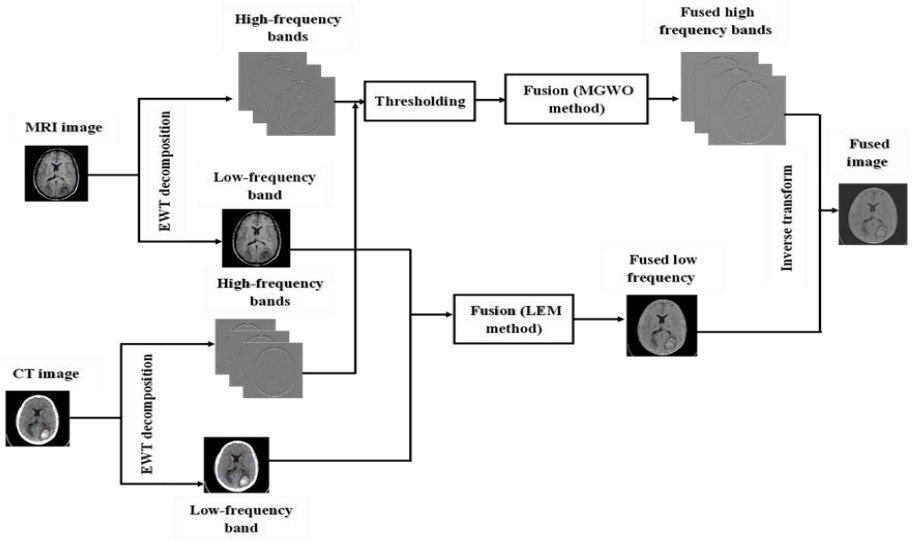

Fig 1. Method for fusing medical images proposed

Though DWT's multi-scale feature has made it popular for application in image fusion, it has some limitations in detecting smoothness along edges and contours. In contrast, MGOA is introduced to prevent the limitation inherent in DWT. Therefore, To get the benefits of MGOA and get around the drawbacks of DWT, the suggested approach combines the two approaches. The recommended medical image fusion technique is depicted sequentially in Figure 1. Fusion of MRI and CT is suggested. The EWT decomposition, LEM integration of low-frequency bands, MGOA integration of high-frequency bands, and inverse wavelet application of the combined image are crucial stages.

3.1. EWT decomposition

Each input image is processed by DWT to extract low- and high-frequency subbands.The source image is shown at a coarser resolution in the low-frequency band. It may be thought of as a downsampled and smoothed version of the original. Consequently, with the low-frequency subband, the majority of the data from the source images is preserved. High-frequency subbands encapsulate the finer details like edges, curves, and region boundaries. Medical images are typically affected by noise during the acquisition process. After decomposition, noise data is present in detailed coefficients. The presence of noise in high-frequency subbands can adversely affect the fusion

process, resulting in unwanted distortions in the fused image. Denoising helps to mitigate these artefacts, producing a more visually pleasing and clinically relevant fused image. By denoising high-frequency subbands before fusion, the fusion image can more accurately represent key features present in MRI and CT scans. This improves diagnostic accuracy, leading to more reliable treatment decisions. Hence, a new thresholding technique is proposed. The proposed threshold function can be expressed as,

$$\widehat{w}_{i,j} = f(x) = \begin{cases} \left(|w_{i,j}| \left(|w_{i,j}| - \frac{T}{\gamma^{\alpha\left(\sqrt{|w_{i,j}|/T-1}\right)}} \right) \right), & |w_{i,j}| < T \\ 0, & |w_{i,j}| \geq T \end{cases} \quad (1)$$

$$T = \sigma_i \frac{\sqrt{2 log n_i}}{\sqrt{n_i}} \quad (2)$$

$$\sigma_i = \frac{MAD(D_i)}{0.6745} \quad (3)$$

$$\text{Mean Absolute Deviation (MAD)} = \text{median}\left(\left|D_j - \text{median}(D_j)\right|\right) \quad (4)$$

Where, α and γ- controlling parameters, n- sub-band image size,σ_i-standard deviation

3.2. Subband fusion

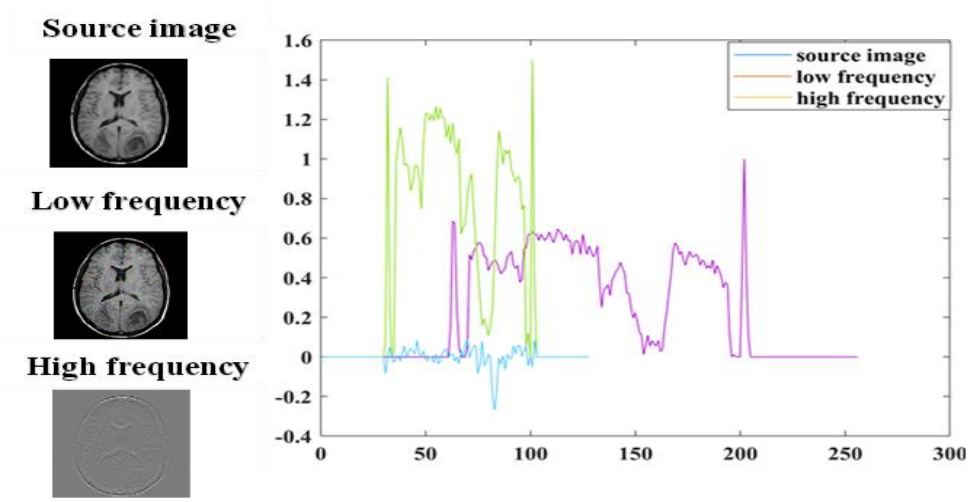

Fig 2. Intensity profile of source image and corresponding low- and high-frequency sub-bands

Figure 2 shows how the various image components' normalized intensities vary. More specifically, a progressive change in pixel intensity is seen in the low-frequency subband, resulting in a smoother appearance compared to the input image while preserving most intensity details. Conversely, the high-frequency subband captures finer details, manifesting in regions where pixel intensity changes occur more rapidly and intensities are lower. Consequently, utilizing unique fusion methods is essential for these subbands to effectively preserve relevant information. Failure to do so may lead to residual artefacts and high contrast. Hence, the proposed method uses unique fusion rules to accommodate the specific characteristics of each subband.

3.2.1. Low-frequency subband fusion

To emphasize and extract pertinent features in the fused image, it is imperative to employ appropriate fusion rules. Several fusing rules including minima, maxima, and averaging, have been extensively investigated for image fusion. Maxima and minima can introduce brightness distortions, and the averaging rule tends to blur the image. To address these concerns. LEM-based fusion rule is adopted in this work. The complete procedure of LEM is outlined in Table.1

Table1.LEM fusion rule

Input: Low-frequency subbands of source images, LF_A, LF_B

Output: Fused low-frequency subband, LF_{AB}

Step1: Compute the local information of LF_A and LF_B

$$LEM_A(x,y) = \sum_{i=1}^{M}\sum_{j=1}^{N}[LF_A(x+i,y+j)]^2 * w(i,j) \quad (5)$$

$$LEM_B(x,y) = \sum_{i=1}^{M}\sum_{j=1}^{N}[LF_B(x+i,y+j)]^2 * w(i,j) \quad (6)$$

$$w(i,j) = \begin{bmatrix}1 & 1 & 1\\ 1 & 1 & 1\\ 1 & 1 & 1\end{bmatrix} \quad (7)$$

Step2: Select the maximum value from the LEM_A and LEM_B local information

$$LI_A(x,y) = \max\{LEM_A(x+i,y+j) | 1 \le i,j \le 3\} \quad (8)$$

$$LI_B(x,y) = \max\{LEM_B(x+i,y+j) | 1 \le i,j \le 3\} \quad (9)$$

Setp3: Compute decision weight maps

$$W_{L1}(x,y) = \begin{cases}1, & if\ LI_A(x,y) > LI_B(x,y)\\ 0, & Otherwise\end{cases} \quad (10)$$

$$W_{L2}(x,y) = \begin{cases}1, & if\ LI_B(x,y) > LI_A(x,y)\\ 0, & Otherwise\end{cases} \quad (11)$$

Setp4: Combine the subbands of low-frequency

$$LF_{AB}(x,y) = w_{L1}(x,y) * LF_A(x,y) + w_{L2}(x,y) * LF_B \quad (12)$$

3.2.2. high-frequency subband fusion

The Grey Wolf Optimization (GWO) algorithm is a novel form of Swarm Intelligence (SI) algorithm, introduced by Mirjalili [22], drawing inspiration from the natural hierarchy and hunting behaviors of grey wolves. The algorithm accomplishes optimization by mathematically replicating the procedures of tracking, encircling, hunting, and attacking that grey wolf populations undergo. The grey wolf's hunting procedure encompasses three key phases: establishment of a social hierarchy, encirclement of the prey, and the actual attack on the prey. Grey wolves, as social canids, occupy a prominent position in the ecological food chain and adhere to a well-defined social structure. Within this hierarchy, the most optimal solution is designated as the alpha (α), followed by the beta (β) and delta (δ) solutions, which represent the next two levels of optimality. The remaining solutions are categorized as omega (ω). The encircling of prey is mathematically represented as follows:

$$\vec{y}(t+1) = \vec{y}_p(t) - \vec{A}.\left|\vec{C}.\vec{y}_p(t) - \vec{y}(t)\right| \quad (13)$$

$$\vec{A} = 2.\vec{a}.r1 - \vec{a} \quad (14)$$

$$\vec{C} = 2.r2 \quad (15)$$

$$\vec{a} = 2 - 2\frac{t}{t_{mx}} \quad (16)$$

The prey and wolf positions are y_p and y, respectively, during the tth iteration. $\vec{A}$ and $\vec{C}$ are coefficient vectors. A is the distance control parameter,$r1$, $r2$ are random values [0,1], and its value decreases from 2 to 0 over the course of iteration, and t_{mx} represents the maximum iteration.

$$\vec{y}_1 = \vec{y}_\alpha - \vec{A}_1.\left|\vec{C}_1.\vec{y}_\alpha - \vec{y}\right| \quad (17)$$

$$\vec{y}_2 = \vec{y}_\beta - \vec{A}_2.\left|\vec{C}_2.\vec{y}_\beta - \vec{y}\right| \quad (18)$$

$$\vec{y}_3 = \vec{y}_\delta - \vec{A}_3.\left|\vec{C}_3.\vec{y}_\delta - \vec{y}\right| \quad (19)$$

$$\vec{y}(t+1) = \frac{\vec{y}_1(t)+\vec{y}_2(t)+\vec{y}_3(t)}{3} \quad (20)$$

Where, $\vec{y}_\alpha$,$\vec{y}_\beta$ and $\vec{y}_\delta$ are the position of the α, β and δ respectively.

Equation (14) reveals that the attenuation factor, directly impacts A, influencing the trade-off between GWO's exploration and exploitation capacity. When a exceeds 1, the grey wolves engage in both searching and hunting activities, while when a is less than 1, they primarily

focus on hunting. In the standard GWO, the distance control parameter demonstrates a linear decrease from 2 to 0 as the number of repetitions increases. However, it is important to note that the individual behavior of the grey wolf during its prey-searching process does not follow a linear pattern. Therefore, the linear reduction of the control parameter does not completely capture the true dynamics of the optimization search process. Equation (14) is replaced by using Equation (21).

$$\vec{a} = 2 * cos\left(\frac{\pi}{2} * \frac{t}{t_{mx}}\right) \quad (21)$$

In this work, by maximizing the fitness function, the MGWO method is utilized to compute the adaptive weights for high-frequency subbands.

3.3. Reconstruction

By using the inverse wavelet transform, the integrated image is reconstructed by using the combined low and high-frequency components.

4. Results and Discussion

This section outlines the experimental configuration, assessment metrics, outcomes, and examination of the suggested approach for combining medical imaging data. The efficacy of the method is confirmed through thorough verification of numerous medical image pairs sourced from the Brain Atlas [8], a Harvard Medical School dataset that is accessible to the general public [8]. For experimental purposes, CT and MRI scans from various diseases are taken from the database. The dataset includes diverse image modalities listed in Table2. Sample images are shown in Figure3.

Notably, all images share the same spatial resolution of 512 X 512 pixels with 256 grayscale levels. The prime objective of this work is to fuse these images to produce fused images imbued with enhanced information content for accurate analysis and diagnosis. which contain more significant information to analyze and make accurate diagnoses. Experiments are conducted using MATLAB on a laptop equipped with an intel® core i5 processor, CPU at 2.4 GHZ with 12 GB RAM, and Windows 11.

Table 2. Details of the medical images used for experimentation

Dataset	No. of images	Type of source images	Disease
Set 1	46	CT-MRI-T1	Fatal stroke
Set 2	52	CT-MRI-T2	Meningioma
Set 3	46	CT-MRI-T1	Sarcoma
Set 4	48	CT-MRI-T2	Speech arrest

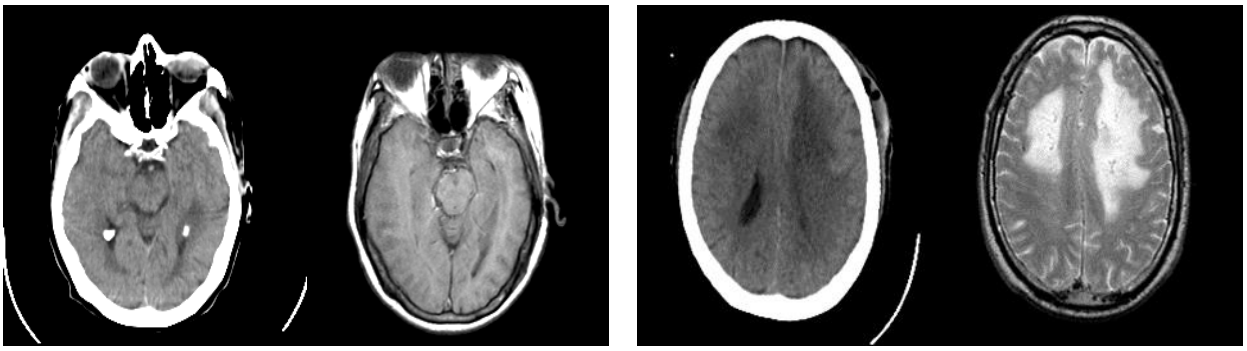

(a) Fatal stroke (b) Meningioma

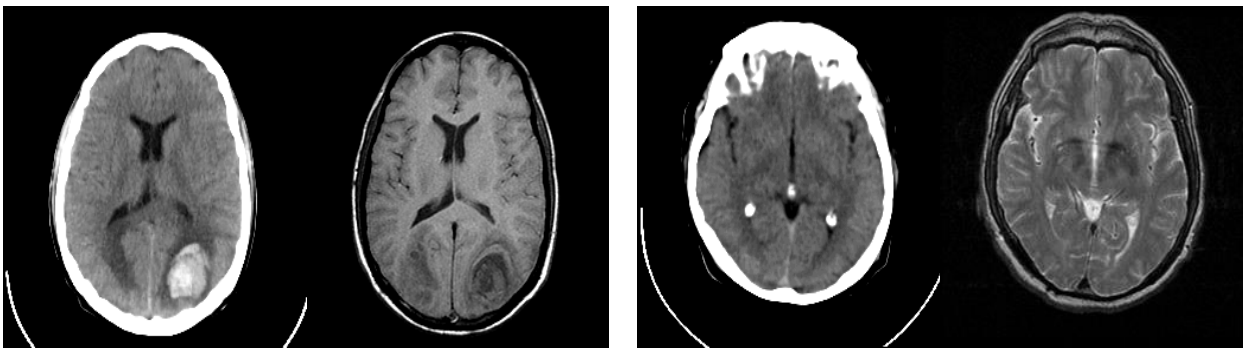

(c) Sarcoma (d)Speech arrest

Fig 3. Sample database: (a) Fatal stroke, (b) Meningioma,(c) Sarcoma, and (d)Speech arrest

4.1. Evaluation metrics

The assessment of image fusion performance primarily revolves around examining the informative attributes transformed from the original images to the combined image that is produced. For quantitative assessment, a few commonly used fusion quality metrics are considered, including Normalized Mutual Information (NMI),Edge intensity (EI), Structural Similarity Index Measure (SSIM), standard deviation (STD),and Correlation (C)[23], [24], [25].

4.2. Result Analysis

The suggested fusion method's efficacy is examined using two distinct approaches: (1) a qualitative study; and (2) a quantitative analysis.

4.2.1.Qualitative analysis

Radiologists see visual inspection as a critical component in evaluating medical image fusion. The dense structures and soft tissue information from the source images should be included in an efficient fusion of CT and MRI images. Figure 4, Figure 5, Figure 6, and Figure 7 depict the visual results of the recommended approach.The first experiment involves the fusion of a CT image and an MRI-TI image of a fatal stroke. The CT scan in Figure4 displays bone structure, while the MRI-T1 scan reveals soft tissue. The fused image in Figure4 presents enhanced anatomical information compared to the individual CT and MRI-T1 images. Remarkably, the essential elements of the CT and MRI-T1 images are effectively preserved in the fused image by the suggested technique.

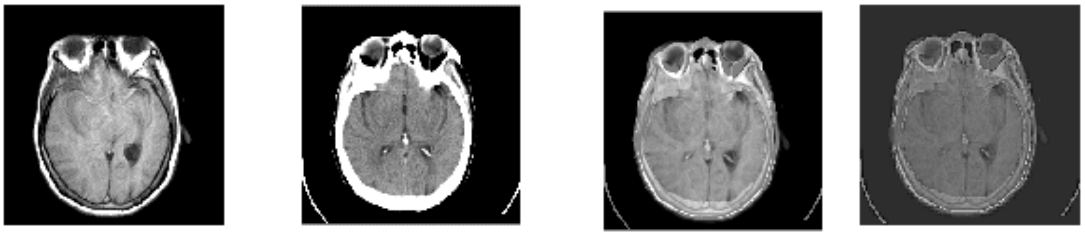

(a)MRI (b)CT (c) NSST-CGWO (d)DWT-PCA

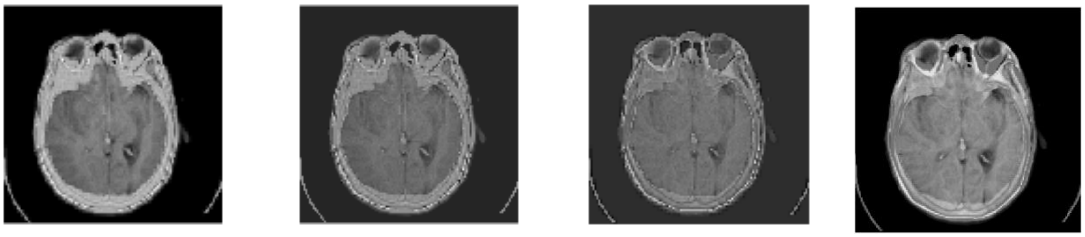

(e)NSST-Xception (f)VMD (g)EJAYA-NSST (h)Proposed

Fig 4. Qualitative outcomes of fatal stroke (CT-MRI-T1)

The second experiment involves examining CT and MRI-T2 images of meningioma. As depicted in Figure 5, CT highlights bone structures, while MRI-T2 offers soft tissue contrast. Fusing these modalities enhances the visualization of both the soft tissue features of the meningioma and its relationship with neighboring bone structures. Additionally, integrating these images to generate a single, higher-quality image is necessary to capture complementary information in a single image, thereby enhancing its utility for clinical diagnosis. Combining the complementary data from both modalities, Figure 5 presents a fused image, resulting in enhanced quality and comprehensive evaluation.

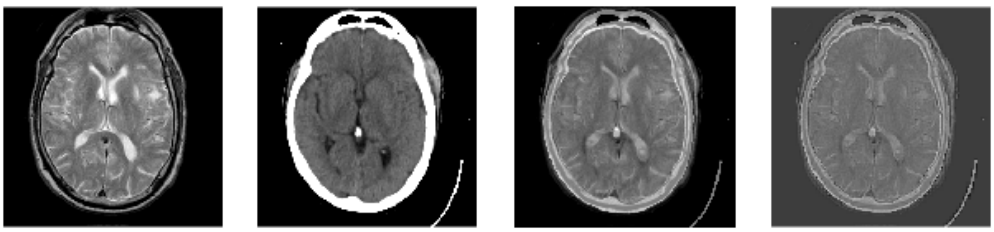

(a)MRI (b)CT (c) NSST-CGWO (d)DWT-PCA

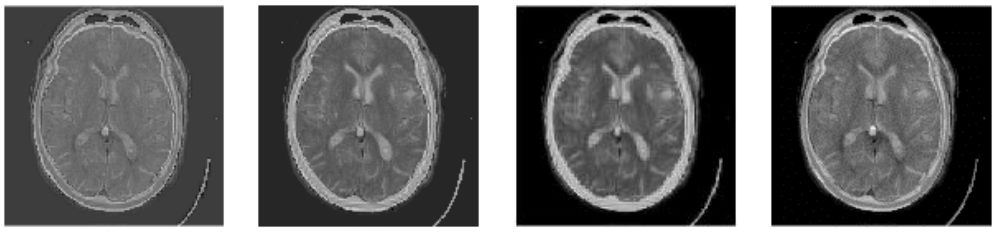

(e)NSST-Xception (f)VMD (g)EJAYA-NSST (h)Proposed

Fig 5. Qualitative outcomes of meningioma (CT-MRI-T2)

The third experiment involves CT and MRI-T1 imaging of sarcoma. The fusion of these modalities presents a pivotal opportunity for accurate identification of the sarcoma, capturing its full extent across bone and soft tissue. This comprehensive visualization not only facilitates precise localization of the sarcoma but also plays a vital role in formulating surgical strategies aimed at minimizing damage to healthy tissues during tumor resection. The resultant fused image in Figure.6, serves as compelling evidence of the efficacy of fusing CR and MRI-T1 images.Notably, the fused version preserved all intricate anatomical details and bone structures, without compromising any pertinent information. This fusion ensures that no crucial details are lost during the fusion process, thereby enabling radiologists to make correct decisions based on a comprehensive and precise representation of the sarcoma's anatomy.

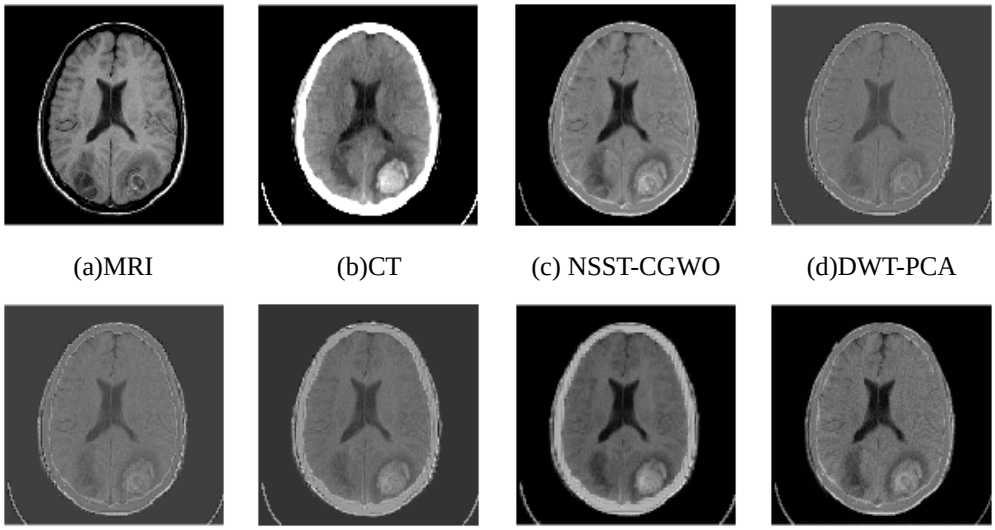

(a)MRI (b)CT (c) NSST-CGWO (d)DWT-PCA

(e)NSST-Xception (f)VMD (g)EJAYA-NSST (h)Proposed

Fig 6. Qualitative outcomes of sarcoma (CT-MRI-T1)

In the fourth experiment,the fusion of CT and MRI-T2 concerning speech arrest is explored. Speech arrest can arise from lesions or abnormalities in various brain regions. Fusing CT and MRI-T2 images allows for precise localization of these lesions within the brain, facilitating accurate diagnosis and treatment planning. Additionally, the fusion of these images enables a more comprehensive characterization of speech arrest. This comprehensive assessment aids in determining the underlying cause of speech arrest and guiding appropriate interventions. Figure7 fused image demonstrated that the suggested approach retained all pertinent data extracted from both modalities, ensuring that no important details are lost in the fusion process.

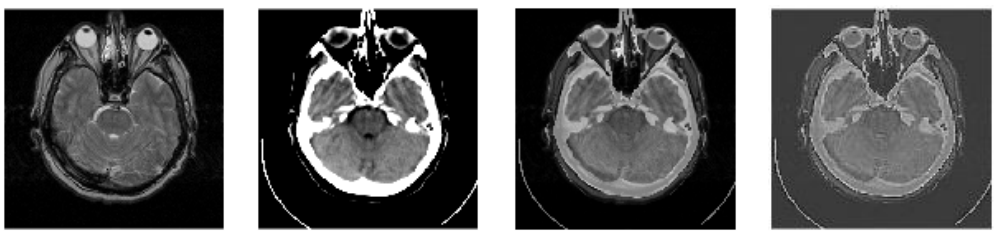

(a)MRI (b)CT (c) NSST-CGWO (d)DWT-PCA

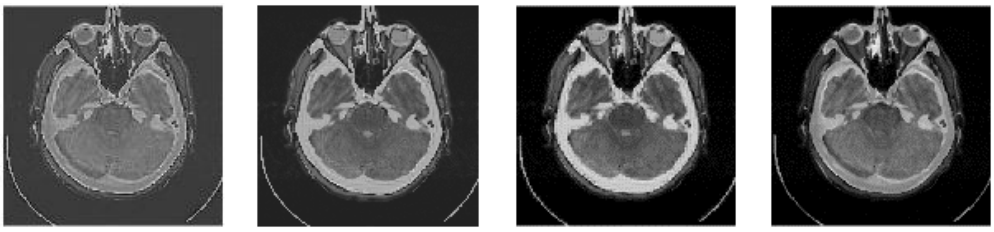

(e)NSST-Xception (f)VMD (g)EJAYA-NSST (h)Proposed

Fig 7. Qualitative outcomes of speech arrest (CT-MRI-T2)

4.2.2. Quantitative Analysis

Using four distinct datasets, several tests were carried out to evaluate the efficacy of the suggested fusion procedure: fatal stroke, meningioma, sarcoma, and speech arrest. Performance comparison was done between the proposed EWT-MGOA and other benchmark models. These models are NSST-CGWO [17], DWT-PCA [18], NSST-Xception [19], VMD [20], and EJAYA-NSST [21]. Quantitative analysis was conducted using various metrics and the outcomes across different fusion techniques are reported in Table3 to Table6 corresponding to each dataset. The overall performance of all images is summarized, with the EWT-MGOA method consistently ranking highest among the compared fusion methods across almost all datasets.

As shown in Table.3, NSST-CGWO exhibited relatively high values for EI and NMI, showing good preservation of edges and similarity to source images. However, its STD, C, and SSIM values are slightly lower compared to the proposed method. DWT-PCA method attained lower values across all metrics compared to other methods, indicating poorer performance compared to other methods. NSST-Xception performed similarly to NSST-CGWO, demonstrating better results in terms of EI and NMI but falls short in other metrics compared to the proposed method. VMD method showed moderate performance across all metrics, with slightly lower values compared to NSST-CGWO and NSST-Xception methods. EJAYA-NSST method performed well but slightly behind NSST-CGWO. All measurements showed that the suggested strategy performed better than any other option. It received the best ratings possible on every parameter, indicating superior performance in preserving edges, retaining information, reducing variability, improving contrast, and maintaining structural similarity.

Table 3. Comparison of quantitative outcomes across various methods for fatal stroke (CT-MRI-T1)

Methods	EI	NMI	STD	C	SSIM
NSST-CGWO	82.76	0.906	68.66	0.855	0.821
DWT-PCA	62.10	0.756	57.19	0.698	0.586
NSST-Xception	70.83	0.838	67.79	0.850	0.715
VMD	64.22	0.803	54.92	0.835	0.661
EJAYA-NSST	76.21	0.849	68.42	0.854	0.717
Proposed	84.84	0.987	71.85	0.973	0.985

As reported in Table4, NSST-CGWO achieved a high EI, suggesting good preservation and enhancement of edges. However when compared to the suggested technique, its NMI, C, STD, and SSIM scores were lower. While the DWT-PCA method yielded moderate scores across all metrics, it lagged in terms of EI, NMI, and SSIM compared to the proposed method. Similarly, NSST-Xception exhibited moderate performance across most metrics. VMD performed well across all metrics, with slight scores compared to the proposed method in terms of EI, NMI, and SSIM. The EJAYA-NSST method demonstrated competitive performance, but its scores were slightly lower compared to the proposed method. Ultimately, the proposed method achieved the highest scores across all metrics, indicating superior performance in preserving edges and maintaining structural similarity compared to other methods. It showed excellent performance compared to other methods in terms of all metrics, making it the most effective choice for fusing CT and MRI-T2 scans for meningioma diagnosis.

Table 4. Comparison of quantitative outcomes across various methods for meningioma (CT-MRI-T2)

Methods	EI	NMI	C	STD	SSIM
NSST-CGWO	80.73	0.893	68.25	0.807	0.753
DWT-PCA	64.51	0.813	55.48	0.726	0.514
NSST-Xception	64.95	0.831	60.35	0.795	0.660
VMD	67.04	0.862	66.77	0.803	0.743
EJAYA-NSST	76.83	0.876	67.11	0.806	0.747
Proposed	85.80	0.986	70.19	0.927	0.949

Table5 highlights that the NSST-CGWO method attained notable EI and NMI values, indicating good edge preservation. However, it showed lower values for other metrics compared to the proposed method. DWT-PCA method displayedthe lowest EI values among all methods, suggesting weaker edge preservation. NSST-Xception showed slightly higher values compared to DWT-PCA for NMI and SSIM. VMD performed well across all metrics, with slightly lower values compared to NSST-CGWO and the proposed method for EI, NMI, and SSIM. EJAYA-NSST achieved good scores for EI, NMI, and SSIM, comparable to NSST-CGWO and VMD. However, its STD and C values were slightly lower compared to the proposed method. When fusion approaches for sarcoma diagnosis were examined, the suggested method performed the best overall. This was achieved by combining CT and MRI-T1. NSST-CGWO and EJAYA-NSST also showed competitive outcomes across some metrics, while DWT-PCA and NSST-Xception appeared to be less effective based on the given evaluation criteria.

Table 5. Comparison of quantitative outcomes across various methods for sarcoma (CT-MRI-T1)

Methods	EI	NMI	STD	C	SSIM
NSST-CGWO	73.42	0.908	60.08	0.800	0.749
DWT-PCA	57.16	0.760	52.48	0.753	0.615
NSST-Xception	58.65	0.834	57.36	0.784	0.640
VMD	60.99	0.827	58.59	0.798	0.711
EJAYA-NSST	71.22	0.857	59.04	0.799	0.718
Proposed	76.45	0.922	62.31	0.915	0.905

As outlined in Table.6,NSST-CGWO achieved moderate to high values for EI,NMI,C,STD, and SSIM, confirming the effective preservation of edges. However, its C and STD values were lower compared to the proposed method. DWT-PCA method showed lower values across all metrics compared to other methods, indicating poor performance. Similarly, the NSST-Xception method also exhibited lower values across all metrics compared to the proposed method, with slightly better values than DWT-PCA for EI,NMI, and SSIM. VMD performed moderately well across all metrics, with relatively higher values compared to DWT-PCA and NSST-Xception. The EJAYA-NSST method achieved moderate to high values for EI,NMI, and SSIM, like NSST-CGWO and VMD. However, its C and STD values are lower compared to the proposed method. The proposed method demonstrated the most superior performance among the compared methods for CT and MRI-T2 fusion for speech arrest diagnosis, with higher values across most evaluation metrics. Other methods showed varying degrees of performance, with NSST-CGWO and VMD also showed competitive results across some metrics. DWT-PCA and NSST-Xception appeared to be less effective based on the given evaluation criteria.

Table 6. Comparison of quantitative outcomes across various methods for speech arrest (CT-MRI-T2)

Methods	EI	NMI	C	STD	SSIM
NSST-CGWO	69.50	1.054	61.62	0.793	0.740
DWT-PCA	53.78	0.864	38.08	0.741	0.510
NSST-Xception	56.68	0.900	46.67	0.781	0.661

VMD	58.31	0.985	60.76	0.789	0.735
EJAYA-NSST	63.93	1.003	61.24	0.790	0.736
Proposed	74.64	0.915	64.94	0.925	0.912

The comparison study clearly shows that for all datasets, the suggested approach continuously performed better across all assessment measures. This confirms the effectiveness of the proposed method in efficiently fusion MRI and CT images while preserving both hard tissue and soft tissue details, thereby enhancing diagnostic accuracy.

5. Conclusion and Future Works

This paper has introduced an innovative framework for multimodal image fusion, using the strengths of both EWT and MGOA. The method improves the robustness of the fusion while circumventing common issues associated with image fusion. By employing the combination of EWT and MGOA, the proposed method exhibits promising outcomes. EWT facilitates time and frequency localization, while the optimization algorithm, MGOA finds adaptive weights for merging high-frequency subbands. Additionally, the integration of low-frequency subbands and the LEM fusion rule further enhances fusion performance by minimizing redundancy, enhancing contrast, and preserving edges.The suggested fusion method's appropriateness for precise and efficient clinical diagnosis is highlighted by a qualitative evaluation of fused images. The quantitative evaluation confirms that the proposed method successfully retains essential features from both source images while also providing complementary information. Comparative analysis reveals that the EWT-MGWO method yields superior outcomes across all metrics. Future research directions could focus on refining feature-level fusion methods.Exploring the application of other metaheuristic algorithms in medical image fusion. Furthermore, investing the potential of machine learning and deep learning approaches in medical image fusion.

Declarations

Data Availability

The corresponding author may provide an image dataset and the code used to support the study's conclusions upon reasonable request.

Source of funding

The study was neither funded, nor was it carried out as a part of employment. The researchers conducted all of the research themselves.

Conflicts of Interest

Conflicts of interest are not disclosed by the authors.

Authors' Contributions

All the authors equally contributed to the research, experimentation, and manuscript writing. All the authors have read and approved the final copy of the manuscript.

References

[1] Algarni, A. D. (2020) Automated medical diagnosis system based on multi-modality image fusion and deep learning, Wire. Pers. Commun., 111, 1033-1058.

[2] Du, I., Li, W., Lu, K., and Xiao, B. (2016) An overview of multi-model medical image fusion, Neuro computing, 215, 3-20.

[3] Zhao, W. and Lu, H. (2017). Medical image fusion and denoising with alternating sequential filter and adaptive fractional order total variation, IEEE trans. Instrum. Meas, 66, 2283-2294.

[4] Hu, Q., Hu, S. and Zhang, F. (2020) Multimodality medical image fusion based on separable dictionary learning and Gabor filtering, signal process. Image communication, 83, 115758.

[5] James, A. P. and Dasarathy (2014) Medical image fusion: A survey of the state of the art, Inf, Fusion, 19, 4-19.

[6] Naidu, V. and Raol, J. (2008). Pixel level image fusion using wavelets and principal component Analysis, Def.Sci. Journal, 58, 338-352.

[7] Haribabu, M. and Bindu, C.H. (2017) Feature level based multimodal medical image fusion with hadamard transforms, International Journal Control Theory Appl., 9(42), 453-460.

[8] Aishwarya, N., Thangammal, C.B. (2018). A novel multimodal medical image fusion using sparse representation and modified spatial frequency. Int. J. Imaging Syst. Technol., 28,175-185.

[9] URL: http://www.med.harvard.edu/aanlib/.

[10] Kong, W., Chen. Y. and Lei, Y. (2021) Medical image fusion using guided filter random walks and spatial frequency in framelet domain. Sig. process., 181, 1079221.

[11] Nie, R., Cao, J., Zhou. D. and Qian, W. (2021) Multi-source information exchange encoding with PCNN for medical image fusion, IEEE Trans. Circuits system. Video Techno, 31, 981-1000.

[12] Kaur. R. and Kaur, E. G. (2015) Medical image fusion using redundant wavelet based ICA co-variance analysis, International Journal. Eng. Comp. sci, 4(8), 28.

[13] Bhateja. V., Patel. H. and Krishna. A. et.al. (2015) Multimodal medical image sensor fusion framework using cascade of wavelet and contourlet transform domains, IEEE sens. Journal, 15, 6783-6790.

[14] Ullah, H., Ullah, B., Wu, L., and Abdulla et al. (2020) Multi-modality medical images fusion based on local features fuzzy sets and novel sum modified Laplacian in non-sampled shearlet transform domain, Biomedical signal process. Control, 57, 101724.

[15] Li, X. and Li, X. (2023) Multimodal brain image fusion based on error texture elimination and slientfeatue detection, Front. NeuroSCi, 17, 1204263.

[16] Kumar,N.N, Prasad,T..J. and Prasad,K.S. (2023). Multimodal medical image fusion with improved multi-objective meta-heuristic algorithm with fuzzy entropy, J. Infor. Know. Management, 22(1),2250063.

[17] Asha, C.S., Lal, S., Gurupur, V.P. and Saxena, P.P. (2019). Multi-modal medical image fusion with adaptive weighted combination of NSST bands using chaotic grey wolf optimization, IEEE Access, 7, 40782–40796.

[18] Tawfik,N., Elnemr,H.A.,Fakhr,M., Dessouky,M.I., Abd El-Samie, F.E. (2021). Hybrid pixel-feature fusion system for multimodal medical images, J. Ambient Intell. Human Comput.,12,6001-6018.

[19] Kaur,M. and Singh,D. (2021). Multi-modality medical image fusion technique using multi-objective differential evolution based deep neural networks. J Ambient Intell. Human Comput., 12, 2483–2493

[20] Polinati, S.,Bavirisetti, D.P., Rajesh, K.N.V.P.S., Naik, G.R. and Dhuli, R. (2021). The fusion of MRI and CT medical images using variational mode decomposition. Appl. Sci., 11, 10975.

[21] Shilpa,S., Rajan,M.R., Asha,C.S. and Shyam,L. (2022). Enhanced JAYA optimization based medical image fusion in adaptive non-subsampled shearlet transform domain. Engg. Sci. Tech. an Int. J., 35,101245

[22] Mirjalili,S., Mirjalili,S.M. and Lewis,A. (2014).Grey Wolf Optimizer, Advances in Engineering Software,69,46-61.

[23] Hempelmann, C.F., Sakoglu, U., Gurupur, V.P. and Jampana, S. (2016). An entropy-based evaluation method for knowledge bases of medical information systems, Expert Syst. Appl., 46, 262–273.

[24] Rick S., Blum. And Zheng, L.(2006). Multi-sensor image fusion and its applications. CRC Press, Taylor & Francis Group, Boca Raton.

[25] Zhang, Y., Jin, M., and Huang, G. (2022). Medical image fusion based on improved multi-scale morphology gradient-weighted local energy and visual saliency map. Biomed. Signal Process. Control 74, 103535